
This is an electronic reprint of the original article.
This reprint may differ from the original in pagination and typographic detail.

Zhu, Hong; Sun, Qinglin; Tao, Jin; Tan, Panlong; Chen, Zengqiang; Dehmer, Matthias; Xie, Guangming

Fluid-Structure Interaction Simulation and Accurate Dynamic Modeling of Parachute Warhead System Based on Impact Point Prediction

Published in:
IEEE Access

DOI:
[10.1109/ACCESS.2021.3099248](https://doi.org/10.1109/ACCESS.2021.3099248)

Published: 26/07/2021

Document Version
Publisher's PDF, also known as Version of record

Published under the following license:
CC BY-NC-ND

Please cite the original version:
Zhu, H., Sun, Q., Tao, J., Tan, P., Chen, Z., Dehmer, M., & Xie, G. (2021). Fluid-Structure Interaction Simulation and Accurate Dynamic Modeling of Parachute Warhead System Based on Impact Point Prediction. *IEEE Access*, 9, 104418-104428. [9493197]. <https://doi.org/10.1109/ACCESS.2021.3099248>

This material is protected by copyright and other intellectual property rights, and duplication or sale of all or part of any of the repository collections is not permitted, except that material may be duplicated by you for your research use or educational purposes in electronic or print form. You must obtain permission for any other use. Electronic or print copies may not be offered, whether for sale or otherwise to anyone who is not an authorised user.

Received June 8, 2021, accepted July 11, 2021, date of publication July 26, 2021, date of current version July 30, 2021.

Digital Object Identifier 10.1109/ACCESS.2021.3099248

Fluid-Structure Interaction Simulation and Accurate Dynamic Modeling of Parachute Warhead System Based on Impact Point Prediction

HONG ZHU¹, QINGLIN SUN¹, JIN TAO^{1,2}, (Member, IEEE),
PANLONG TAN¹, ZENGQIANG CHEN¹, MATTHIAS DEHMER³,
AND GUANGMING XIE⁴, (Member, IEEE)

¹College of Artificial Intelligence, Nankai University, Tianjin 300350, China

²Department of Electrical Engineering and Automation, Aalto University, 02150 Espoo, Finland

³Department of Computer Science, Swiss Distance University of Applied Sciences, 3900 Brig, Switzerland

⁴College of Engineering, Peking University, Beijing 100871, China

Corresponding author: Jin Tao (taoj@nankai.edu.cn)

This work was supported in part by the National Natural Science Foundation of China under Grant 61973172, Grant 61973175, Grant 62003175, and Grant 62003177; in part by the National Key Research and Development Project under Grant 2019YFC1510900; in part by the Key Technologies Research and Development Program of Tianjin under Grant 19JCZDJC32800; in part by the China Postdoctoral Science Foundation under Grant 2020M670633; and in part by the Academy of Finland under Grant 315660.

ABSTRACT To predict a parachute–warhead system’s dynamic characteristics and impact point, numerical methods are used to comprehensively predict the large deformations of the parachute during the opening process and the impact point of the system in the terminal landing phase. Fluid–structure interaction simulations based on the arbitrary Lagrangian–Eulerian method are used to study the Disk–Gap–Band parachute’s inflation behavior and provide the parachute’s aerodynamic parameters at steady state. Based on the obtained aerodynamic data, a nine-degree-of-freedom dynamic model of the parachute–warhead system was established, which was used to predict the landing area of the system by calculating the falling trajectory. Based on the established model, an online impact point prediction program was developed. Finally, the effectiveness and accuracy of the methods were verified by airdrop experiments. The results showed that the methods for the parachute–warhead system modeling during the inflation and terminal descent phases could effectively predict its dynamic characteristics, which could be further applied for precision airdrop missions.

INDEX TERMS Parachute–warhead system, parachute inflation, impact point prediction, multibody dynamics.

I. INTRODUCTION

Theoretical research and system design of parachute systems are essential in the application of flexible aircraft. Parachutes are mainly used for the deceleration and stabilization of payloads. Due to their diversity and convenience, parachute systems have been applied in the fields of spacecraft recovery, emergency rescue, and cargo airdrops [1]–[3].

Although both parachutes and paragliders are flexible aircraft, their operating characteristics are quite different. The parafoil system has been extensively studied due to its

controllability and good gliding performance [4]–[6]. The parachute system is subjected to wind fields without control mechanisms, so accurate dynamic modeling is important for predicting the performance of a parachute system.

The parachute–warhead system utilizes the parachute to decelerate. Owing to the lightweight of the parachute, its motion is easily influenced by the airflow. Therefore, the drop zone of the warhead will be shifted under the wind field, which will affect the arrangement of the warhead damage detection sensor and increase the difficulty of test data acquisition. To make the parachute–warhead system fall into the effective detection range of the sensors during the testing, it is necessary to accurately predict the impact point of the

The associate editor coordinating the review of this manuscript and approving it for publication was Hassen Ouakad¹.

warhead before deployment [7]. Consequently, establishing a reliable impact point prediction program is of great significance for the development of parachute–warhead systems for precise airdrop capabilities.

There has been much research on the prediction of the projectile impact point. Yuan *et al.* [8] put forward a tracker to compensate for the influence of wind. Montenbruck *et al.* [9] predicted the instantaneous ballistic impact point of unpowered airdrop based on GPS data. On the basis of radar measurement technology, Ravendra *et al.* [10], [11] acquired the approximate kinematic parameters for the projectile. In addition, many studies on the trajectory planning and landing guidance for the unpowered airdrop phase have been conducted [12]–[14].

An accurate dynamics model is a prerequisite for the impact point prediction of a parachute–warhead system. The dynamics model can simulate the trajectory and dynamic behavior of the parachute system to reduce the number of expensive and time-consuming experiments [15], [16]. For different research purposes, three-degree-of-freedom (DOF), six-DOF, nine-DOF, or higher-DOF dynamics models can be established for the parachute payload system [17]–[19]. Harlin and Cicci [20] built a six-DOF dynamic model of ballistic missile by iterating the state transition matrix in the falling process. The simulation results showed that the relative motion between parachute and payload changed the equilibrium state of the system and the flight path and impact point. By considering relative motion, Jung and Hwang [21], Song and Han [22] introduced multiple-model interaction algorithms for space vehicles. These algorithms combined multiple models to describe the dynamic characteristics of the research objects.

However, the complex and time-varying behaviors of flexible fabric structures result in a complicated unsteady flow of the surrounding fluid, which brings challenges to the design of a parachute system. The unsteady behaviors manifest as a large number of separated flows, strong nonlinear fluid–structure interaction (FSI) coupling, and unsteady wakes. To achieve the equilibrium states, the canopy geometry needs to change dramatically under highly nonlinear responses. The magnitude and direction of the pressure load are functions of the parachute shape and cannot be determined in advance. In the prior dynamic modeling process, the calculation of aerodynamic parameters was often idealized, and the strong couplings between the flexible parachute and the surrounding fluid flow were not included. To accurately predict the aerodynamics of parachutes, FSI methods were adopted in this paper to simulate the flexible structure behavior and predict the aerodynamic performance of a parachute. Based on the obtained aerodynamic forces, an accurate dynamics model was further established to predict the parachute–warhead system’s landing point.

Several effective methods have been developed to analyze the dynamic characteristics of parachute systems. Stein [23] examined the unfolding behavior of the parachute on the basis of the fully coupled FSI method, which made a vital advance

in the numerical simulation of parachutes. But the only disadvantage was that the computing cost was expensive. In order to improve calculation capability, Tutt and Taylor [24] applied the Eulerian–Lagrangian penalty coupling algorithm and the multi-material arbitrary Lagrangian–Eulerian (ALE) method to research the dynamics of the parachute unfolding process. The ALE fluid–structure coupling method was also used for the Disk–Gap–Band (DGB) parachute, which proved that the DGB parachute had a strong ability to resist overload [25]–[28]. Therefore, in the damage detection experiment of the warhead, the DGB parachute was used to decelerate the warhead. In addition to the large deformation of the parachute in the opening process, the dynamic characteristics of the parachute–warhead system in the steady descent phase should also be important for the final landing [29], [30].

In this paper, dynamic simulations were conducted to reproduce the dynamic behaviors of the parachute–warhead system in the operating stages of inflation and terminal landing. Based on the previous work of parachute infinite mass opening simulations under numerical wind tunnel experiment conditions [31], the finite mass simulations under low-speed airdrop conditions were further carried out, which were more close to the parachute opening process of the actual experiment. The FSI simulations used the most advanced ALE method and finite element method, which simulated the opening process of the canopy and provided a prediction of the aerodynamic loads acting on the canopy after the parachute reached steady state. Furthermore, the visualizations of the structure shape and flow field distribution provided knowledge of the physical phenomenon and modifications of related parameters. This paper establishes a high-fidelity nine-DOF dynamic model of the parachute–warhead system based on the obtained aerodynamic parameters to predict its impact point online. The methods were applied in two airdrop experiments, and both airdrops reached the target conditions, indicating that the proposed methods were effective and feasible.

The remaining sections of the paper are organized as follows. The numerical methods for the FSI simulations are described briefly in Section II. In Section III, the nine-DOF dynamic model of the parachute–warhead system is presented. The simulation results of the parachute inflation are given in Section IV, and the results of airdrop experiments are shown in Section V to verify the proposed model of the parachute–warhead system for impact point predictions. Finally, the conclusions of this work are presented in Section VI.

II. FSI MODEL OF PARACHUTE INFLATION PROCESS

The opening of the parachute canopy is a highly nonlinear and complex time-varying process [24]. The correct inflation of the canopy is a prerequisite for the valid function of the warhead. However, it is difficult to obtain the aerodynamic load distributions on the parachute affected by nonlinear FSI characteristics. Accurate modeling of the parachute–warhead system can facilitate the study and prediction of the

TABLE 1. Structural parameters of the parachute.

Parameter	Value
Nominal Diameter (m)	2.72
Rope Length (m)	2.72
Diameter of top-hole (m)	0.56
Number of ropes	24

system’s performance. Therefore, the accurate calculation of aerodynamics has a key influence on the accuracy of the dynamic model. To better understand the dynamic characteristics of the parachute and obtain the aerodynamic value of the strong coupling between the parachute and the airflow, this section introduces the FSI simulation method of the DGB parachute, whose geometric parameters are consistent with those of the parachute used in the airdrop experiments (see Table 1).

A. MATHEMATIC MODEL

The parachute system is a low-speed flexible aircraft, and the surrounding air can be considered incompressible [26]. Therefore, the governing equations of the fluid in the entire domain Ω_f can be described as:

$$\rho \left(\frac{\partial \mathbf{u}_f}{\partial t} + \mathbf{u}_f \cdot \nabla \mathbf{u}_f + \mathbf{f}_f \right) - \nabla \cdot \boldsymbol{\sigma}_f = 0 \quad \text{on } \Omega_f, \quad (1)$$

where \mathbf{u}_f is the velocity of the fluid, \mathbf{f}_f is the body force, $\boldsymbol{\sigma}_f$ is the Cauchy stress tensor, and ρ is the air density.

The governing equation of the structural domain Ω_s is

$$\rho_s \frac{\partial \mathbf{u}_s}{\partial t} = \boldsymbol{\sigma}_s(\mathbf{u}_s) + \rho_s \cdot \mathbf{f}_s \quad \text{on } \Omega_s, \quad (2)$$

where \mathbf{u}_s is the structural displacement vector, \mathbf{f}_s is the external force, $\boldsymbol{\sigma}_s$ is the Cauchy stress tensor, ρ_s is the material density.

The solid elements with the advantage of momentum convection are suitable for solving the Navier-Stokes equations of fluid. The second-order van Leer monotonic upstream-centered scheme for conservation laws (MUSCL) was utilized to calculate the variable values in the transport fluxes to achieve accurate second-order monotonic results. And the projection method was used for fluid to decouple the discrete velocity-pressure equations. In order to effectively solve the values of pressure and velocity that satisfy the continuity equation, a split-step method proposed by Gresho was adopted in this paper. Please refer to [32] for more details about this method.

B. FINITE ELEMENT MODEL

Since the inflation performance of the parachute is directly affected by the quality of the folding method of the canopy, the initial geometric shape of the parachute in the numerical simulation determines the prediction results of the parachute-warhead system. In this paper, we study the process from the moment that the canopy is deployed. Therefore, only lateral

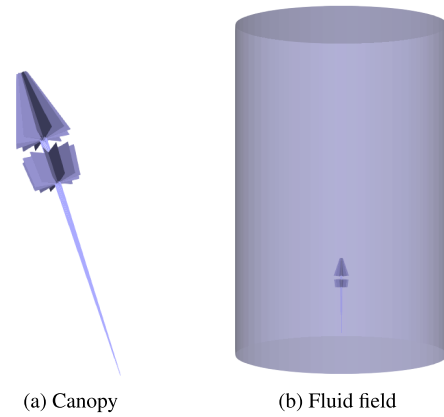


FIGURE 1. Computer-aided design (CAD) model of infinite mass inflation of parachute.

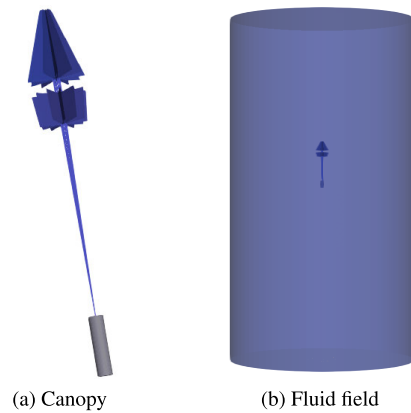


FIGURE 2. CAD model of finite mass inflation of parachute.

folding is considered. The FSI simulations of the parachute opening process were carried out under the conditions of wind tunnel experiments (infinite mass condition) and airdrop experiments (finite mass condition). The computer-aided design (CAD) models are shown in Fig. 1 and 2. The geometric size and weight of the payload in the finite mass inflation process simulation of the parachute were constructed based on the actual airdrop experiment. The dimensions of the flow field should be large enough to ensure that there are no wall effects on the canopy. Based on the CAD models, finite element models were obtained by mesh generations for the next FSI simulations, as shown in Fig. 3. The canopy was discretized by quadrilateral grids, and the flow field was discretized by hexahedral grids. Capturing the complex fluid dynamic patterns requires the quite small grids, so the size of fluid grids around the canopy is generally smaller than the structure grids of the canopy. Correspondingly, the finer the grids, the more accurate the calculations, at the same time, the more expensive the computing costs. Therefore we need to make a trade-off between the resolution of the grids and the accuracy. The flow field elements near the canopy were refined, and the larger the distance from the canopy was,

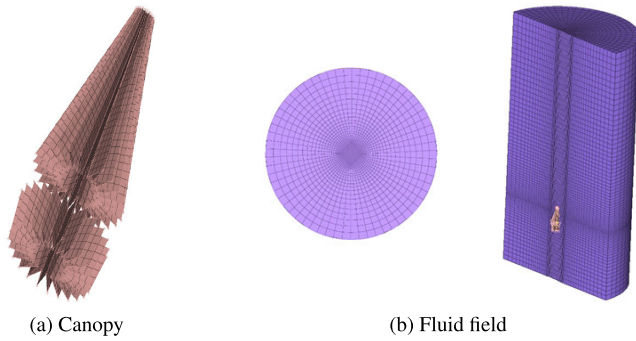


FIGURE 3. Mesh models of parachute inflation simulation.

the bigger the element size to ensure the calculation accuracy while reducing the computational cost was.

C. Eulerian–Lagrangian PENALTY FUNCTION METHOD

In the process of FSI simulation, data transfer was required between the structural domain and the fluid domain. First, the fluid domain calculated the initial pressure loads on the canopy surface under the initial canopy boundary conditions, and then passed it on to the structure domain to calculate the deformation of the canopy under the initial aerodynamic loads. When the calculations tended to converge, the new boundary conditions were transferred to the fluid domain. In this way, the final structural shape and aerodynamic loads of the parachute can be obtained until the results of both the fluid domain and structure domain were no longer changed.

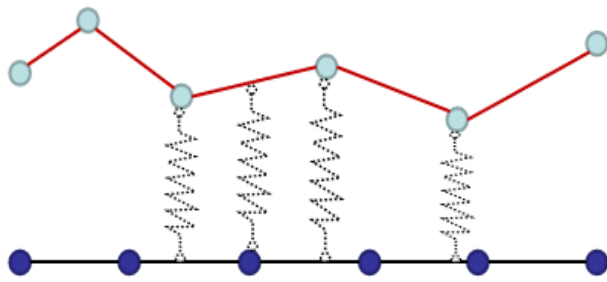


FIGURE 4. Schematic diagram of eulerian–lagrangian penalty function method.

In this paper, the data transfer between the fluid domain and the structure domain was carried out by the Eulerian–Lagrangian penalty function method. At the beginning of each time step, the fluid solver first checked whether there were penetrations between the slave nodes of the structural domain and the master nodes of the fluid domain. If there were penetrations, a series of spring-like contact forces were introduced between the slave nodes and the main surfaces and between the master nodes and the slave surfaces, so the penetrations were limited by the contact depth and contact

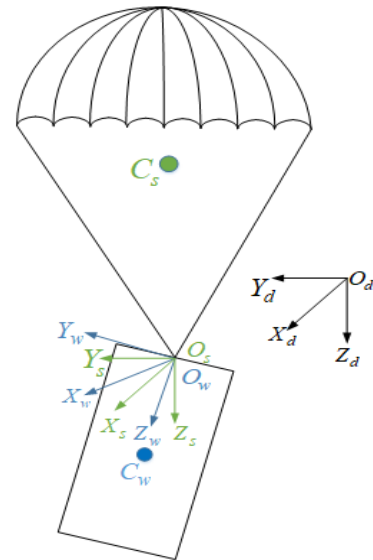


FIGURE 5. Schematic diagram of the coordinate systems.

stiffness. This is called the penalty function. The schematic diagram of this process is shown in Fig. 4.

III. DYNAMIC MODEL OF TERMINAL DESCENT PHASE

To predict the impact point of the warhead accurately, a multi-body dynamics model was established. The parachute and warhead were considered to be two independent components that were connected by a hinge joint.

Before modeling, the following reasonable assumptions were made to facilitate the analysis.

- The elasticity of the suspension lines is negligible.
- The canopy is axisymmetric. After inflating, it resembles a hemisphere.
- The aerodynamic pressure center of the parachute coincides with its gravity center.
- The aerodynamic forces and the moments of the warhead are neglected.
- The ground is a horizontal plane.

The three main right-handed coordinate systems used in the parachute–warhead system modeling are shown in Fig. 5. The two coordinate systems with the origins at the connection point of parachute and warhead were the warhead frame $O_w X_w Y_w Z_w$ and the canopy frame $O_s X_s Y_s Z_s$. The subscripts w and s represent the warhead and parachute canopy, respectively. The axis $O_w Z_w$ pointed to the mass center of the warhead, and the axis $O_w Y_w$ pointed to the right side of the warhead. The axis $O_s Z_s$ pointed downward, and the axis $O_s Y_s$ was perpendicular to $O_s Z_s$ and pointed to the right side of the canopy. The origin of the geodetic frame was at a fixed point in space. The axis $O_d X_d$ pointed to the North, the axis $O_d Y_d$ pointed to the East, and the axis $O_d Z_d$ pointed vertically downward. Based on the above coordinate systems, we described the acting forces of the canopy and the warhead

in their coordinate frames, respectively. And the conversions of these two coordinate frames to the geodetic coordinate frame were completed by the conversion matrix described by the yaw angle ψ , the pitch angle θ , and the roll angle ϕ .

$$T_{d-s} = \begin{bmatrix} c\theta c\psi & c\theta s\psi & -s\theta \\ s\zeta s\theta c\psi & s\zeta s\theta s\psi + c\zeta c\psi & s\zeta c\theta \\ c\zeta s\theta c\psi & c\zeta s\theta s\psi - s\zeta c\psi & c\zeta c\theta \end{bmatrix}, \quad (3)$$

where $\cos(*) = c*$, $\sin(*) = s*$.

In the airdrop experiment of the parachute-warhead system, the dynamic model is a basis for the accurate prediction of impact points. Due to the dynamic characteristics of the parachute are quite different during inflating and steady descending phases, the dynamic model of the whole working process should be established by stages. Considering the relative motions between the parachute and the warhead, this paper established a nine-DOF dynamic model to accurately predict the locations of the landing points.

A. DYNAMICS EQUATIONS OF WARHEAD

The dynamic governing equations of the system can be obtained according to the theorem of momentum and moment of momentum. The velocity and angular velocity of the warhead were represented by V_w and A_w , respectively. The momentum Q_w and moment of momentum M_w in the warhead coordinate system were expressed as follows:

$$\begin{bmatrix} Q_w \\ M_w \end{bmatrix} = J_w \begin{bmatrix} V_w \\ A_w \end{bmatrix} \quad (4)$$

where J_w denotes the generalized mass matrix of the warhead. The geometry of the warhead is a homogeneous cylinder with a height of h_w , a bottom radius of r_w , and a mass of m_w . According to the generalized inertia matrix in theoretical mechanics, the detailed expressions of J_w were obtained as

$$J_w = \begin{bmatrix} J_{w1} & J_{w2} \\ J_{w3} & J_{w4} \end{bmatrix} \quad (5)$$

$$J_{w1} = \begin{bmatrix} m_w & 0 & 0 \\ 0 & m_w & 0 \\ 0 & 0 & m_w \end{bmatrix}, \quad (6)$$

$$J_{w2} = J_{w1} R^T [L_{Ow}] J_{w1}, \quad (7)$$

$$J_{w3} = R [L_{Ow}] J_{w1}, \quad (8)$$

$$J_{w4} = I_w + R^T [L_{Ow}] J_{w1} R [L_{Ow}], \quad (9)$$

$$I_w = \begin{bmatrix} \frac{1}{12} m_w (3r_w^2 + h_w^2) & 0 & 0 \\ 0 & \frac{1}{12} m_w (3r_w^2 + h_w^2) & 0 \\ 0 & 0 & \frac{1}{2} m_w r_w^2 \end{bmatrix}, \quad (10)$$

where L_{Ow} represents the position vector from the mass center of the warhead to the origin of the warhead coordinate system. $R[\cdot]$ is an antisymmetric matrix:

$$R[(x \ y \ z)] = \begin{bmatrix} 0 & -z & y \\ z & 0 & -x \\ -y & x & 0 \end{bmatrix}. \quad (11)$$

According to the linear momentum and angular momentum theorems, we obtained

$$\begin{aligned} \frac{\partial Q_w}{\partial t} + A_w \times Q_w &= J_{w1} \dot{V}_w + J_{w2} \dot{A}_w \\ &\quad + A_w \times (J_{w1} V_w + J_{w2} A_w) \\ &= F_w^G + F_T, \quad (12) \\ \frac{\partial M_w}{\partial t} + V_w \times Q_w + A_w \times M_w &= J_{w3} \dot{V}_w + J_{w4} \dot{A}_w \\ &\quad + V_w \times (J_{w1} V_w + J_{w2} A_w) \\ &\quad + A_w \times (J_{w3} V_w + J_{w4} A_w) \\ &= M_w^G + M_T, \quad (13) \end{aligned}$$

where F_w^G represents the vector of the gravity of the warhead in the warhead coordinate system, and M_w^G represents the torque resulted from the gravity. F_T represents the pulling force of the ropes on the warhead, and M_T represents the moment that resulted from the pulling force.

B. DYNAMIC EQUATIONS OF PARACHUTE

Since the parachute is lightweight and the enclosed volume is large when it is fully deployed, the average density of the parachute is close to the air density. Therefore, the influence of apparent mass must be considered [33]. We use V_s and A_s to represent the velocity and angular velocity of the mass center of the parachute in the canopy coordinate system, then the momentum Q_s and moment of momentum M_s of the parachute can be expressed as

$$\begin{aligned} \begin{bmatrix} Q_s \\ M_s \end{bmatrix} &= [M_a + M_r] \begin{bmatrix} V_s \\ A_s \end{bmatrix} = \begin{bmatrix} M_1 & M_2 \\ M_3 & M_4 \end{bmatrix} \begin{bmatrix} V_s \\ A_s \end{bmatrix} \\ &= \begin{bmatrix} M_1 V_s + M_2 A_s \\ M_3 V_s + M_4 A_s \end{bmatrix}, \quad (14) \end{aligned}$$

where M_a and M_r represent the apparent mass and the real mass of the parachute respectively. M_1, M_2, M_3, M_4 are the components of the total mass matrix. The specific forms are as follows.

$$M_a = \begin{bmatrix} a_1 & 0_{3 \times 3} \\ 0_{3 \times 3} & a_4 \end{bmatrix}, M_r = \begin{bmatrix} r_1 & r_2 \\ r_3 & r_4 \end{bmatrix}, \quad (15)$$

$$r_1 = \begin{bmatrix} m_s & 0 & 0 \\ 0 & m_s & 0 \\ 0 & 0 & m_s \end{bmatrix}, \quad (16)$$

$$r_2 = (r_1 + a_1) R^T [L_{Os}], \quad (17)$$

$$r_3 = R [L_{Os}] (r_1 \ a_1), \quad (18)$$

$$r_4 = I_s + R^T [L_{Os}] (a_1 + r_1) R [L_{Os}], \quad (19)$$

$$I_s = \text{diag} \begin{bmatrix} \frac{1}{3} m_s (R_0^2 + H_0^2) - m_s (0.163 D_0)^2 \\ \frac{1}{3} m_s (R_0^2 + H_0^2) - m_s (0.163 D_0)^2 \\ \frac{2}{3} m_s R_0^2 \end{bmatrix}, \quad (20)$$

The shape of the fully inflated parachute is similar to a hemisphere. In Eq. (20), R_0 represents the diameter of the horizontal projection circle, and H_0 represents the height of the vertical projection. The governing equations of the

parachute were also obtained from the linear momentum and angular momentum theorem.

$$\begin{aligned} \frac{\partial Q_s}{\partial t} + A_s \times Q_s &= M_1 \dot{V}_s + M_2 \dot{A}_s + A_s \\ &\quad \times (M_1 V_s + M_2 A_s) \\ &= F_s^G + F_{-T} + F_{aero}, \end{aligned} \quad (21)$$

$$\begin{aligned} \frac{\partial M_s}{\partial t} + V_s \times Q_s + A_s \times M_s &= M_3 \dot{V}_s + M_4 \dot{A}_s \\ &\quad + V_s \times (M_1 V_s + M_2 V_s) + A_s \\ &\quad \times (M_3 V_s + M_4 A_s) \\ &= M_s^G + M_{-T} + M_{aero}, \end{aligned} \quad (22)$$

where F_s^G is the gravity of the parachute and ropes described in the parachute coordinate system, F_{aero} is the aerodynamic force on the parachute, and F_{-T} is the pulling force of warhead on ropes. M_s^G , M_{aero} , and M_{-T} are the corresponding moments.

C. DYNAMIC CONSTRAINTS

Since the parachute–warhead system is hinged, the attitude angles of the parachute and the warhead are independent of each other. However, the velocities at the connection point O_s of the parachute and the warhead are equal, that is, the velocities of V_s and V_w at O_s have the following constraints in the parachute coordinate system $O_s X_s Y_s Z_s$ and the warhead coordinate system $O_w X_w Y_w Z_w$.

$$V_s = T_{d-s} T'_{d-w} V_w, \quad (23)$$

Similarly, the pulling force of the parachute to the warhead and that of the warhead to the parachute are a pair of forces and reactions at the connection point O_s , with equal magnitude and opposite direction. According to the nature of the acting force and reaction force, we have:

$$F_{-T} + T_{d-s} T'_{d-w} F_T = 0. \quad (24)$$

The nine-DOF dynamic model of the parachute–warhead system is composed of Eqs. (12), (13), (21), (22), (23), and (24).

IV. SIMULATION RESULTS OF PARACHUTE INFLATING

Considering the deceleration characteristics of the parachute–warhead system during the opening process, the inflation of the parachute can be classified into infinite mass and finite mass conditions. Specifically, the deceleration can be neglected during the infinite mass inflation process of parachute in wind tunnel experiments. On the contrary, the deceleration of the system is obvious during finite mass inflation of parachutes in airdrop testing. In this paper, based on the high-performance scalability of the MPP ability of the LS-DYNA R8 solver, the FSI simulations for the parachute inflation process were conducted in parallel on a workstation with a large number of CPUs, which greatly improved the computational efficiency.

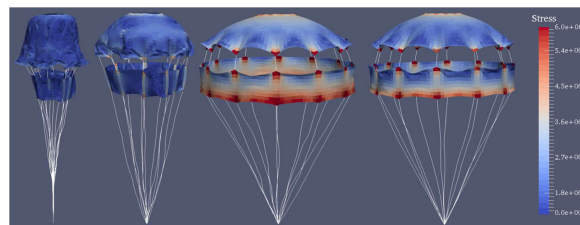


FIGURE 6. Infinite mass inflation process of parachute (the time from left to right is 0.08, 0.15, 0.24, and 0.35 s).

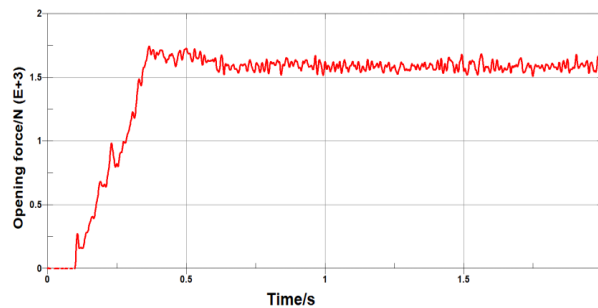
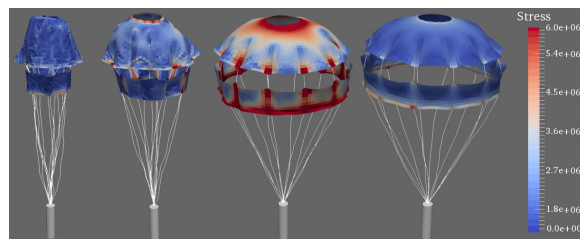
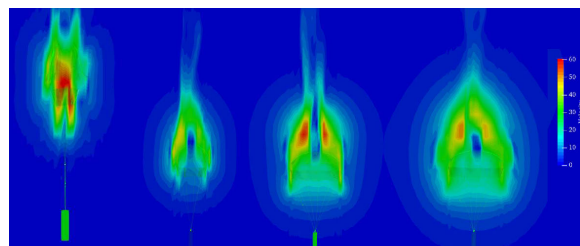


FIGURE 7. Change of opening force.



(a) Deformation shape with stress contours of canopy surface



(b) Velocity contours of central symmetric cross section

FIGURE 8. Infinite mass inflation process of parachute (the time from left to right is 0.15, 0.24, 0.35, and 0.48 s).

A. INFINITE MASS INFLATION

Fig. 6 shows the deformation process of the DGB parachute under the infinite mass inflation conditions with the fixed end of the ropes. It can be seen from the figure that when the parachute started to inflate from the initial straightening state, the airflow first entered the canopy from the bottom, causing the lower part of the canopy to expand rapidly. As the airflow continued to accumulate, the air gradually filled the upper part of the canopy, making the canopy like a microphone shape. Then the canopy continued to open entirely. Due to the instantaneous impact force, the canopy reached the maximum

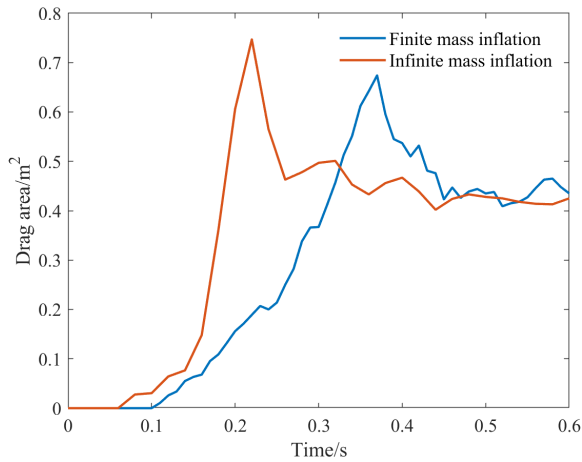
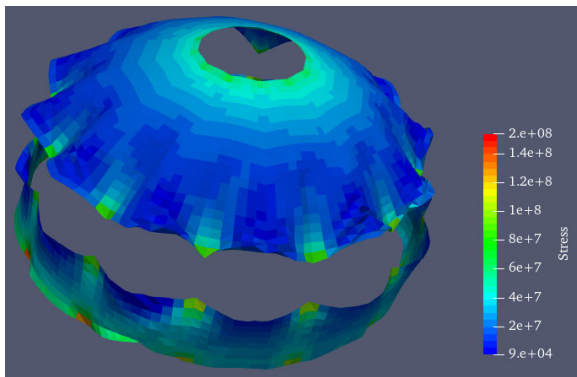
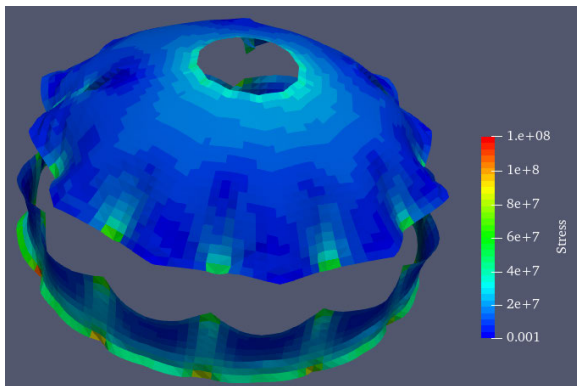


FIGURE 9. Canopy projected area verse time.



(a) Infinite mass inflation



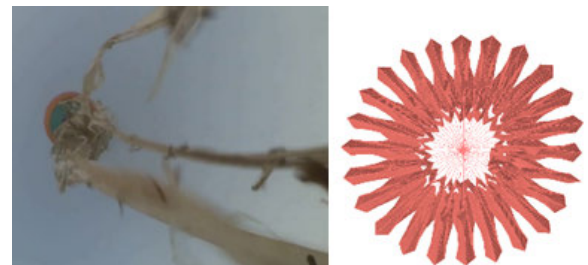
(b) Finite mass inflation

FIGURE 10. Stress contour of canopy.

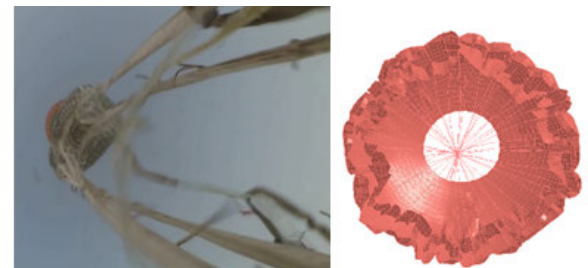
inflated shape during the inflation process, and the local force on the surface also arrived at the highest. This can also be seen from the changing curve of the parachute opening force shown in Fig. 7, the opening force attained a peak value of 1740 N at 0.365 s, and then the value gradually converged, finally the opening force stabilized at about 1600 N. The fluctuations in the steady state corresponded to the breathing phenomenon of the canopy in the actual working process.



(a) t = 0s



(b) t = 0.12s



(c) t = 0.32s



(d) t = 0.6s

FIGURE 11. Comparison of parachute deformation shape between simulation and airdrop experiment.

As a result, the FSI simulation completely described the deformations of the parachute and aerodynamic load distributions during inflation.

B. FINITE MASS INFLATION

Fig. 8 shows the variation of the canopy shape with time and the corresponding velocity contours of the central cross section in the case of a finite mass inflation. Fig. 8a shows that the deformation process of the canopy during inflation was similar to that of the infinite mass inflation case, but it took longer to reach the final opening. In addition, the formation and dissipation of the vortex cores around the canopy are



(a) Precision airdrop system by hot-air balloon



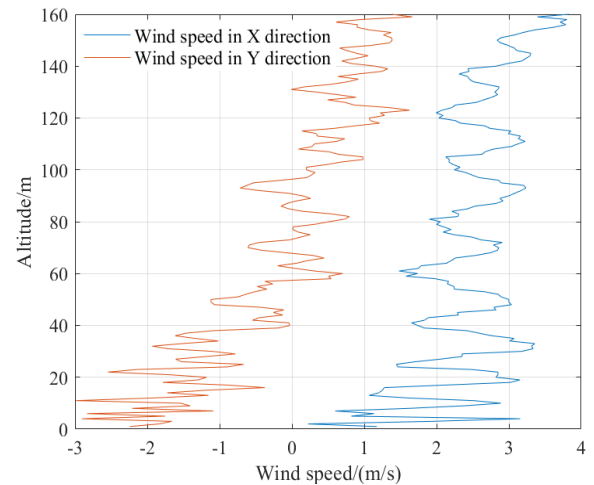
(b) Ground station

FIGURE 12. Airdrop testing.

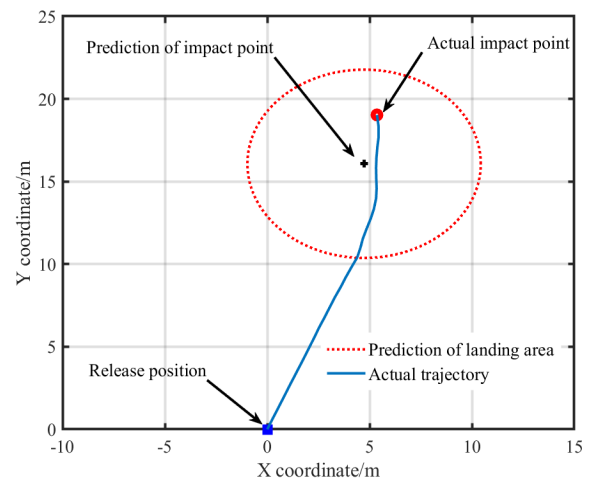
shown in Fig. 8b. At first, the airflow entered the interior of the canopy and formed a vortex, and as the canopy expanded, it then moved outside through the top hole to the upper part of the canopy and split into two symmetric vortex cores, after which it disappeared gradually.

Fig. 9 shows the variation of the projected area of the parachute under the conditions of a finite mass inflation and infinite mass inflation. We can see that the times for the parachute to reach the maximum projected area under infinite and finite mass inflation conditions were 0.22 and 0.37 s, respectively, with a delay of about 0.15 s under the finite mass inflation conditions. The decrease in the parachute opening speed may have been due to the effects of gravity and the extra drag induced by the payload. Therefore, the operating environment has a significant influence on the parachute inflating performance.

The von Mises stress response of the canopy under aerodynamic pressure is shown in Fig. 10. After the parachute was fully inflated and reached a steady state, the stress



(a) Wind field



(b) Impact point prediction results

FIGURE 13. Airdrop test 1.

distributions on the canopy surfaces between infinite and finite mass inflation conditions were not significantly different. The stresses near the top hole and the edges of the canopy were relatively high, especially at the positions connecting with the ropes. Reinforcing belts should be arranged at these positions to prevent the canopy from tearing or damage.

V. EXPERIMENTAL RESULTS

A. PARACHUTE INFLATION PHASE

Fig. 11 shows the comparison of the canopy deformation shapes over time between the numerical simulation and the airdrop test during inflation, which proved that the simulation results reproduced the canopy inflation process accurately. In the airdrop test, the time for the canopy to reach steady state after inflation was about 0.42 s, which was consistent with the results of the parachute finite mass inflation simulation.

B. IMPACT POINT PREDICTION PHASE

Based on the dynamic models of the parachute inflation phase and stable descent phase established in Sections II and III,

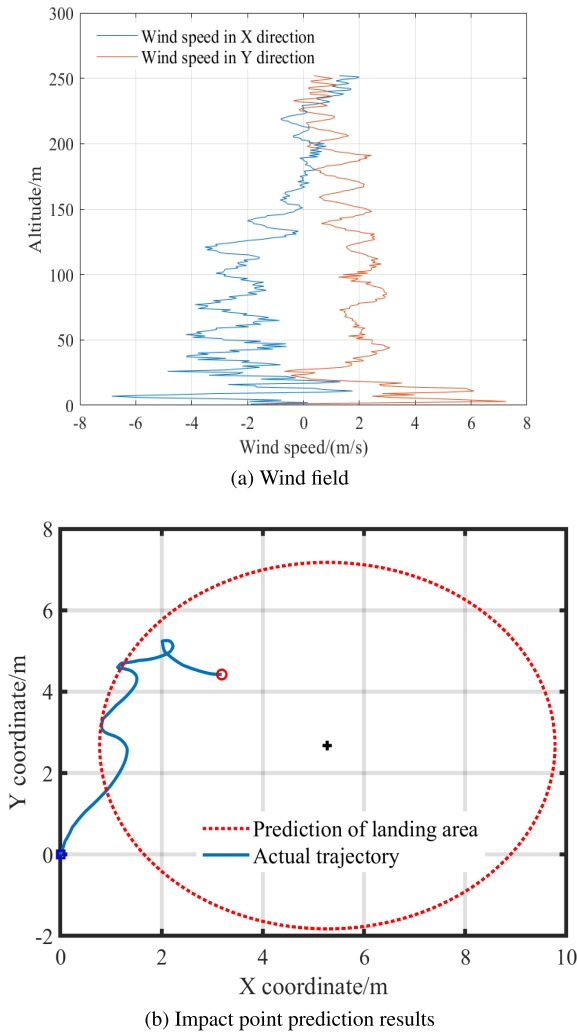


FIGURE 14. Airdrop test 2.

a landing point prediction program of the parachute-warhead system was constructed, as shown in Fig. 12. The landing point prediction program was executed at the ground station. The data transmission module transmitted the GPS and wind field data through hot-air balloon airdrop equipment. The ground station used the current GPS position of the airdrop system to predict the range of the landing area to obtain a target circle. The airdrop was carried out when the coincidence area between the predicted target circle and the predefined landing area reached 80%. Two airdrop experiments were carried out at different altitudes to verify the established impact point prediction system. The detailed parameters and results of the airdrop experiments are given in Table 2.

Figs. 13 and 14 present the actual changes of the wind field with height and the airdrop landing prediction results of the two airdrop experiments. The X and Y directions in the figure refer to the longitude and latitude directions, respectively. The red dotted line was the predicted target circle, the red dot was the actual landing point, and the black dot was the

TABLE 2. Experimental data and results of airdrop tests.

Experiment number	1	2
Release height (m)	146	251
Falling time (s)	6.19	9.4
Parachute opening time (s)	0.47	0.48
Prediction radius (m)	6	4.5
Prediction error (m)	3.35	2.72

center of the predicted target circle, which was considered to be the predicted impact point. The distances between the final impact points and the predicted impact points of two airdrop tests were 3.35 and 2.72 m, respectively, which were within the acceptable error range. The error may have resulted from data measurement errors and parachute opening process errors without considering the influence of the wind field. The above results proved the effectiveness and feasibility of the dynamic models and prediction algorithms established in this paper.

VI. CONCLUSION

There is great potential for improving the prediction accuracy of the impact point of a parachute-warhead system by precise dynamic modeling. The dynamic behaviors of the parachute-warhead system were studied by combining the numerical methods of the FSI simulation and dynamic modeling. The numerical simulations of the inflation process of the DGB parachute were carried out by the FSI method, incorporating the ALE and finite element methods. The structural and aerodynamic characteristics of the parachute system during inflation under infinite mass and finite mass conditions were studied. The results showed that the opening environments had a significant influence on the inflation time. Based on the obtained aerodynamic parameters, an accurate nine-DOF dynamic model of the parachute-warhead system was established, which overcomes the inherent defects of traditional modeling methods due to the simplifications of the aerodynamic model. Furthermore, a ground station program for predicting the landing point of the parachute-warhead system online was developed based on real-time wind field and GPS data. The airdrop experiments demonstrated that the prediction results were in good agreement with the actual drop points, indicating that the proposed methods can provide a high fidelity simulation tool for applying precise parachute-warhead airdrop systems.

REFERENCES

- [1] R. A. Mach-Egrave, C. S. Iacomini, J. M. Stein, and C. J. Cerimele, "Flight testing the parachute system for the space station crew return vehicle," *J. Aircr.*, vol. 38, no. 5, pp. 786–799, Sep./Oct. 2001.
- [2] T. Bennett and R. Fox, "Design, development & flight testing of the NASA X-38 7500 ft2 parafoil recovery system," in *Proc. 17th AIAA Aerodyn. Decelerator Syst. Technol. Conf. Seminar*, Reston, VA, USA: American Institute of Aeronautics and Astronautics, 2003, p. 2107.
- [3] T. W. Knacke, *Parachute Recovery Systems Design Manual*. Santa Barbara, CA, USA: Para Publishing, 1991.
- [4] P. Tan, M. Sun, Q. Sun, and Z. Chen, "Dynamic modeling and experimental verification of powered parafoil with two suspending points," *IEEE Access*, vol. 8, pp. 12955–12966, 2020.

- [5] J. Tao, M. Dehmer, G. Xie, and Q. Zhou, "A generalized predictive control-based path following method for parafoil systems in wind environments," *IEEE Access*, vol. 7, pp. 42586–42595, 2019.
- [6] J. Tao, Q. Sun, H. Sun, Z. Chen, M. Dehmer, and M. Sun, "Dynamic modeling and trajectory tracking control of parafoil system in wind environments," *IEEE-ASME Trans. Mechatron.*, vol. 22, no. 6, pp. 2736–2745, Dec. 2017.
- [7] J. T. Vandermeij, D. B. Doman, and A. R. Gerlach, "Release point determination and dispersion reduction for ballistic airdrops," *J. Guid., Control, Dyn.*, vol. 38, no. 11, pp. 2227–2234, 2015.
- [8] T. Yuan, Y. Bar-Shalom, P. Willett, and D. Hardiman, "Impact point prediction for thrusting projectiles in the presence of wind," *IEEE Trans. Aerosp. Electron. Syst.*, vol. 50, no. 1, pp. 102–119, Jan. 2014.
- [9] O. Montenbruck, M. Markgraf, W. Jung, B. Bull, and W. Engler, "GPS based prediction of the instantaneous impact point for sounding rockets," *Aerosp. Sci. Technol.*, vol. 6, no. 4, pp. 283–294, Jun. 2002.
- [10] V. C. Ravindra, Y. Bar-Shalom, and P. Willett, "Projectile identification and impact point prediction," *IEEE Trans. Aerosp. Electron. Syst.*, vol. 46, no. 4, pp. 2004–2021, Oct. 2010.
- [11] V. C. Ravindra, Y. Bar-Shalom, and P. Willett, "Impact point prediction and projectile identification," in *Signal and Data Processing of Small Targets*, vol. 6699. San Diego, CA, USA: SPIE, 2007, pp. 66991A-1–66991A-10.
- [12] C. A. Kluever, "Unpowered approach and landing guidance," *J. Guid., Control, Dyn.*, vol. 27, no. 6, pp. 967–974, 2004.
- [13] X.-J. Lan, L. Liu, and Y.-J. Wang, "Online trajectory planning and guidance for reusable launch vehicles in the terminal area," *Acta Astronautica*, vol. 118, pp. 237–245, Jan. 2016.
- [14] C. A. Kluever and C. A. Neal, "Approach and landing range guidance for an unpowered reusable launch vehicle," *J. Guid., Control, Dyn.*, vol. 38, no. 11, pp. 2057–2066, Mar. 2015.
- [15] K.-F. Doherr and H. Schilling, "Nine-degree-of-freedom simulation of rotating parachute systems," *J. Aircr.*, vol. 29, no. 5, pp. 774–781, Sep. 1992.
- [16] V. N. Dobrokhodov, O. A. Yakimenko, and C. J. Junge, "Six-degree-of-freedom model of a controlled circular parachute," *J. Aircr.*, vol. 40, no. 3, pp. 482–493, May 2003.
- [17] S. Herrington, J. Renzelman, T. Fields, and O. Yakimenko, "Modeling and control of a steerable cruciform parachute system through experimental testing," in *Proc. AIAA Scitech Forum*, Jan. 2019, p. 1074.
- [18] J. R. Cruz, D. Way, J. Shidner, J. L. Davis, R. W. Powell, D. Kipp, D. S. Adams, A. Sengupta, A. Witkowski, and M. Kandis, "Parachute models used in the Mars science laboratory entry, descent, and landing simulation," in *Proc. AIAA Aerodyn. Decelerator Syst. (ADS) Conf.*, Mar. 2013, p. 1276.
- [19] P. R. Schatzle and W. H. Curry, "Flight simulation of a vehicle with a two-stage parachute system," *J. Aircr.*, vol. 17, no. 8, pp. 545–546, Aug. 1980.
- [20] W. J. Harlin and D. A. Ciccini, "Ballistic missile trajectory prediction using a state transition matrix," *Appl. Math. Comput.*, vol. 188, no. 2, pp. 1832–1847, May 2007.
- [21] J.-K. Jung and D.-H. Hwang, "The novel impact point prediction of a ballistic target with interacting multiple models," in *Proc. 13th Int. Conf. Control, Automat. Syst. (ICCAS)*, Oct. 2013, pp. 450–453.
- [22] H. Song and Y. Han, "Comparison of space launch vehicle tracking using different types of multiple models," in *Proc. 19th Int. Conf. Inf. Fusion (FUSION)*, 2016, pp. 209–216.
- [23] K. Stein, R. Benney, V. Kalro, T. E. Tezduyar, J. Leonard, and M. Accorsi, "Parachute fluid-structure interactions: 3-D computation," *Comput. Methods Appl. Mech. Eng.*, vol. 190, nos. 3–4, pp. 373–386, 2000.
- [24] B. Tutt and A. Taylor, "The use of LS-DYNA to simulate the inflation of a parachute canopy," in *Proc. 18th AIAA Aerodyn. Decelerator Syst. Technol. Conf. Seminar*, May 2005, pp. 56–64.
- [25] X. Gao, Q. Zhang, and Q. Tang, "Parachute dynamics and perturbation analysis of precision airdrop system," *Chin. J. Aeronaut.*, vol. 29, no. 3, pp. 596–607, Jun. 2016.
- [26] X. Gao, Q. Zhang, Q. Tang, and T. Yang, "Fluid-structure interaction simulation of parachute in low speed airdrop," in *Proc. World Congr. Eng.*, vol. 3, 2013, pp. 1923–1928.
- [27] X. Gao, Q. Zhang, and Q. Tang, "Fluid-structure interaction analysis of parachute finite mass inflation," *Int. J. Aerosp. Eng.*, vol. 2016, pp. 1–8, Jan. 2016.
- [28] Y. Li, C. Jiang, L. Mao, and M. Li, "Study on transient dynamics and aerodynamic characteristics of a new type of high-damping four-winged rotating parachute inflation process," *Math. Problems Eng.*, vol. 2020, pp. 1–20, Mar. 2020.
- [29] M. B. Quadrelli, J. M. Cameron, and V. Kerzhanovich, "Multibody dynamics of parachute and balloon flight systems for planetary exploration," *J. Guid., Control, Dyn.*, vol. 27, no. 4, pp. 564–571, Jul. 2004.
- [30] G. Guglieri, "Parachute-payload system flight dynamics and trajectory simulation," *Int. J. Aerosp. Eng.*, vol. 2012, pp. 1–17, Jan. 2012.
- [31] H. Zhu, Q. Sun, J. Han, and Z. Chen, "Numerical simulation and experiment for impact point prediction of parachute-warhead system," in *Proc. 39th Chin. Control Conf. (CCC)*, Jul. 2020, pp. 1221–1226.
- [32] P. M. Gresho, "On the theory of semi-implicit projection methods for viscous incompressible flow and its implementation via a finite element method that also introduces a nearly consistent mass matrix. Part 1: Theory," *Int. J. Numer. Methods Fluids*, vol. 11, no. 5, pp. 587–620, Oct. 1990.
- [33] T. Yavuz, "Determining and accounting for a parachute virtual mass," *J. Aircr.*, vol. 26, no. 5, pp. 432–437, May 1989.



HONG ZHU received the B.E. degree from Henan Ploytechnic University, Henan, China, in 2017. She is currently pursuing the Ph.D. degree with Nankai University, Tianjin. Her current research interests include computational fluid dynamics of flexible aircraft, fluid–structure interactions, and active disturbance rejection control.



QINGLIN SUN received the B.E. and M.E. degrees in electrical engineering and automation from Tianjin University, Tianjin, China, in 1985 and 1990, respectively, and the Ph.D. degree in controlling science and engineering from Nankai University, Tianjin, in 2003.

He is currently a Professor with the Intelligence Predictive Adaptive Control Laboratory and the College of Artificial Intelligence, Nankai University. His current research interests include self-adaptive control, modeling and control of flexible spacecraft, complex systems, and embedded control systems and their applications.



JIN TAO (Member, IEEE) received the B.Sc. degree in automation from the Qingdao University of Science and Technology, Qingdao, China, in 2008, the M.Sc. degree in control theory and control engineering from the Guangxi University of Science and Technology, Liuzhou, China, in 2011, and the Ph.D. degree in control science and engineering from Nankai University, Tianjin, China, in 2017. He is currently an Associate Professor with the College of Artificial Intelligence,

Nankai University. He is also associated with the Department of Electrical Engineering and Automation, Aalto University. He has published more than 50 peer-reviewed articles in international journals and conferences. His research interests include intelligent control, evolutionary optimization, and multiagent systems.



PANLONG TAN received the B.S. and M.S. degrees in automation and control theory and control engineering from the Tianjin University of Technology, Tianjin, China, in 2010 and 2013, respectively, and the Ph.D. degree in control science and engineering from Nankai University, Tianjin, in 2016. He is currently a Postdoctoral Researcher with the College of Artificial Intelligence, Nankai University. His current research interests include active disturbance rejection control and the modeling and control of flexible spacecraft.



ZENGQIANG CHEN received the B.S., M.E., and Ph.D. degrees from Nankai University, in 1987, 1990, and 1997, respectively. He is currently a Professor in control theory and engineering with Nankai University and the Deputy Director of the Institute of Robotics and Information Automation. His current research interests include intelligent predictive control, chaotic systems and complex dynamic networks, and multi-agent system control.



MATTHIAS DEHMER received the B.Sc. degree in mathematics from the University of Siegen, Germany, in 1997, and the Ph.D. degree in computer science from the Darmstadt University of Technology, Germany, in 2005. He is currently a Full Professor with the Swiss Distance University of Applied Science, Brig, Switzerland, and the UMIT—The Health and Life Sciences University, Tirol, Austria. He has authored and coauthored more than 250 publications. His H-index is 39 and

his i10-index is 127. His research interests include data science, cybersecurity, disaster management, complex networks, risk analysis, information systems, machine learning, information theory, bioinformatics, visual analytics, and computational statistics.



GUANGMING XIE (Member, IEEE) received the B.S. degree in applied mathematics and electronic and computer technology and the M.E. and Ph.D. degrees in control theory and control engineering from Tsinghua University, Beijing, China, in 1996, 1998, and 2001, respectively.

From 2001 to 2003, he was a Postdoctoral Research Fellow with the Center for Systems and Control, Department of Mechanics and Engineering Science, Peking University, Beijing, China.

In 2003, he joined the Center as a Lecturer. He is currently a Full Professor in dynamics and control with the College of Engineering, Peking University. His research interests include smart swarm theory, multiagent systems, multirobot cooperation, biomimetic robot, switched and hybrid systems, and networked control systems.

Dr. Xie is an Associate Editor of *Scientific Reports*, the *International Journal of Advanced Robotic Systems*, *Mathematical Problems in Engineering*, and an Editorial Board Member of the *Journal of Information and Systems Science*.

• • •